CORROSION SCIENCE AND TECHNOLOGY, Vol.17, No.2(2018), pp.60~67
[Research Paper]
pISSN: 1598-6462 / eISSN: 2288-6524
DOI: https://doi.org/10.14773/cst.2018.17.2.60

Detection of Iron Phases Presents in Archaeological Artifacts by Raman Spectroscopy

A. L. Barbosa†, C. Jimenez, and J. A. Mosquera

University of Cartagena, Science Faculty, Chemistry Department, Laboratory of Catalysis research and New materials, LICATUC, Pharmacy Building, Campus de Zaragocilla, Cartagena-Colombia South America

(Received September 08, 2017; Revised March 29, 2018; Accepted April 18, 2018)

The compounds associated with corrosion, in metallic archaeological samples of carbon steel of insular origin were evaluated to establish their degree of deterioration and structural damage against air pollution. The iron phases present in samples of archaeological artifacts were detected by Raman spectroscopy and confocal Raman microcopy. These samples mainly exhibited ing mainly β-FeO(OH) type goethite oxyhydroxides and small amounts of akaganeite α-FeO(OH) lepidocrocite γ-FeO(OH) due to dominant chloride in a marine environment and non-stoichiometric oxyhydroxides Fe (II + / III +) as indicators of early corrosion. Some parts showed the presence of magnetic maghemite indicating high corrosion. γ-FeO(OH) is a precursor of phases associated with advanced marine corrosion. By studying its decomposition by Raman spectroscopy, it was synthesized with the following sequence: γ-FeO(OH) → α-FeO(OH) + γ-FeO(OH), →γ–Fe_2O_3+ Fe_3O_4. Ferric compounds provided evidence for the effect of intensity of laser on them, constituting a very useful input for the characterization of oxidation of iron in this type of artifacts. Thus, destructive analysis techniques should be avoided in addition to the use of small amounts of specimen.

Keywords: *Iron oxyhydroxides, Marine corrosion, Ferroalloys, Lepidocrocite, Metallic heritage samples*

1. Introduction

It had been estimated that the expenses damages due attributed to corrosion represent between 3 and 5 percent of the gross domestic product of the industrialized countries GNP; only talking about steel, for every ten tons manufactured per year, two and a half are lost due to the effects of corrosion [1]. Some authors [2-5] have studied the corrosion products of carbon steels in various atmospheres by DRX, SEM and Raman, reporting as main phases present lepidocrocite γ-FeO(OH), goethite α-FeO(OH), akaganeite β–FeO(OH) and magnetite (Fe_3O_4), As shown in (Fig. 1), the presence of these iron compounds constitute a timeline in the materials, which facilitate a diagnosis of the progress of the corrosion of a metal part. The lepidocrocite phase is associated with the first stages of atmospheric corrosion [2] and is the starting point to form more aggressive phases, so synthesize it and analyze its decomposition by Raman spectroscopy, monitoring the signals a 219 cm^{-1},252 cm^{-1} and 650 cm^{-1} is relevant. This iron oxyhydroxide is very sensitive to the conditions of synthesis even under conditions of strict control; it presents small morphological changes [6]. The γ -FeO (OH) phase can be transformed into the polymorphic goethite phase α-FeO(OH) with gentle heating [7,8]. If it is calcined at temperatures close to 250 °C it becomes maghemite γ -Fe_20_3, losing structural water and changing the paramagnetic to ferromagnetic phase [9,10-12], this phase shows an aggressive corrosion phenomenon and the surface of the part he barely recovers. Later oxidation leads to compounds such as magnetite and hematite α-Fe_20_3 [7] causing rupture and total loss of the material, being irrecoverable. In this work we study the compounds associated with corrosion, in metallic archaeological samples of carbon steel of insular origin and that were buried, to establish their degree of deterioration and structural damage against air pollution. The phase of lepidocrocite was synthesized, [9], studying its thermal stability by Laser Raman spectroscopy, monitoring the signals 219 cm^{-1},252 cm^{-1} and 650 cm^{-1}.

2. Experimental Methods

2.1 Selection of the study area and sampling

The archaeological artifacts were collected in the Battery

† Corresponding author: abarbosal@unicartagena.edu.co

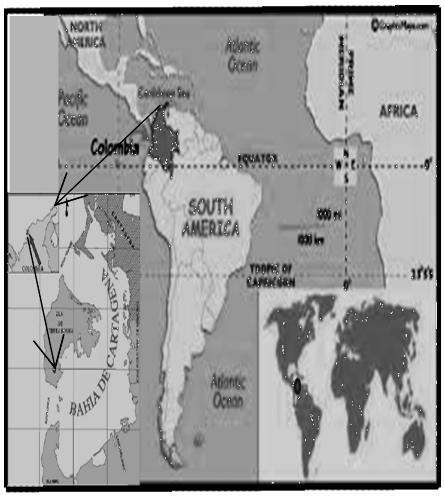

Fig. 1 Location "Land pump" island, -Cartagena Colombia-South America.

Fig. 2 Sampling areas in each of the metal artillery parts.

of San Rafael Angel, located on the island "Land pump", in the northern zone of the Bay of Cartagena-Colombia-South America, latitude: 10°19' 44.1 N "and longitude: 75°34' 48.9 O", (Fig. 1). Samples were taken from 8 parts of cannons, located the right and left side of the San Rafael Battery, coded as C1 to C8, (Fig. 4). Each canyon was studied by optical microscopy, and Raman spectroscopy, in three zones along the part (head indicated with black, yellow half body and part of the red tip), (Fig. 2). The confocal Raman microscopy, (Fig. 3), was used in the yellow zone. Under the desquamated material that showed poor adherence, a metallic matrix was found, used to quantify the Fe wt% of each part, using an atomic absorption equipment, brand:Thermo, Model: ICE3000 A A05124605 v1,30.

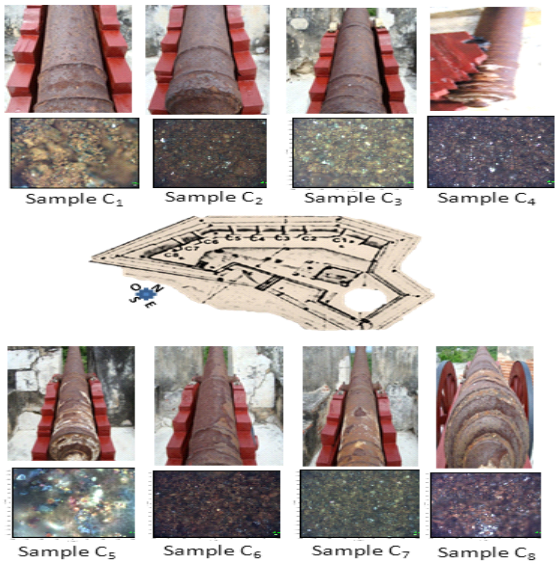

Fig. 3 Pieces of artillery C1-C8 taken in latitude: 10° 19 '44.1 N "and longitude: 75° 34' 48.9 O". Battery of San Rafael Angel Cartagena Colombia-South America.

2.2 Raman analysis

In most cases the corrosion crusts, partially detached from the archaeological samples, were used, in other cases it was made by speculation by sieving them and passing them through a 40 mesh screen. These were analyzed, for initial characterization, by the use of a stereomicroscope optical microscope, Nikon model: C-LEDS with magnification lenses of 0.88, 1.60 and 3.5 for each sample. In addition to use Nikon confocal microscope model BX41, with objectives of 50X and 100X achromatic plane, color video camera for vision of the sample, coupled to the Raman with He / Ne laser of λ = 633 nm and 25 mW, for the analysis of the the average zone of the samples, the acquisition and data processing was used the Software Labspec under windows. For the study of compounds associated with corrosion. Two Laser Raman teams were employed. The first equipment (Horman Jobin Yvon confocal Raman spectrometer, Labram HR High Resolution Model), with Renishaw Ramanscope InVia system, which allowed the focused laser tip to scan in two spatial dimensions (xyy) on the sample, with one step of 1 μm. The measurements were carried out in air using the He-Ne excitation line of λ = 633 nm, with a power of the laser source was 25 mW, which was attenuated to the minimum value allowed by the instrument, up to 0.24 mW in order to avoid structural transformations of the iron phases by the action of the laser that occur when the power in the sample is higher than 0.7 mW [6]. A second Raman team (Dimension-P1 Raman System with excitation source

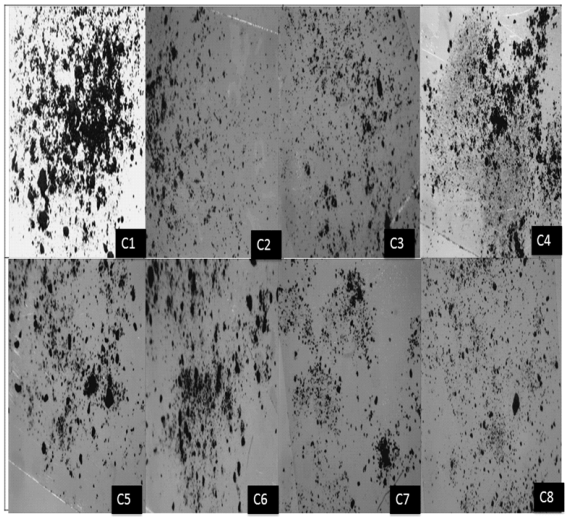

Fig. 4 Initial visual analysis, Stereomicroscope optical microscope, Nikon model: C-LEDS with 3.5 magnification lenses.

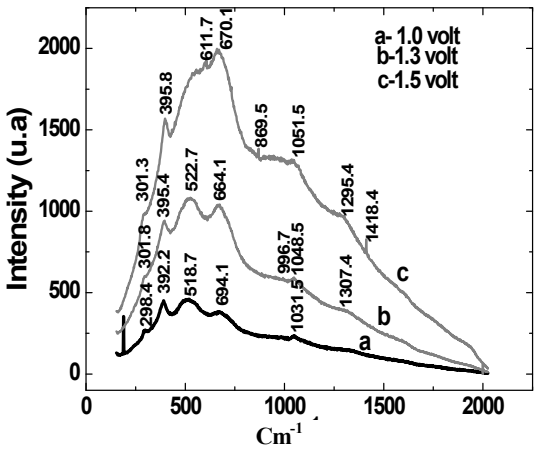

Fig. 5 Profile Raman spectrum of synthesized lepidocrocite γ-FeO(OH), versus several voltage applied to the laser.

Diode Laser, operating in the near infrared (785.27 nm), using CCD detector of 1.340 x 100 imaging pixels, 20 x 20 μm, in a range of 200 cm^{-1}- 3300 cm^{-1} Resolution 4 cm^{-1} -5 cm^{-1} (2.5 cm^{-1} / pixel), a power of the laser source was 216.3 mW and data acquisition system One-step acquisition / prediction using chemometric methods, was used for stability studies of lepidocrocite γ FeO(OH), in which vary the voltage applied to the laser.

2.3 Synthesis of lepidocrocite

It was carried out with the addition of 20 ml of Fe $(NO_3)_3.9H_2O$ 1M and changing the OH^-/ Fe^3 + ratio (changes in pH), with additions of 5M NaOH with final relation OH^- / Fe^{3+} de 0.5, 0.75 and 1.5 [13], the variation of this parameter had a clear effect on the crystallization of the different phases of iron oxyhydroxides.

3. Results and Discussion

The visual analysis carried out on the artillery artifacts, shows desquamated corrosion products in the body of the pieces, as can be seen on the (Fig. 3). Pittings was observed in all the pieces C1-C8, by interperism, with the appearance of colored spots of orange on the surface of the cannons C1, C3, C4, C5, C7 and C8. For pieces C4, C5 and C8 a greater advance of corrosion along its entire length is shown, possibly due to its position in the San Rafael battery place and composition of corrosive phases such as magnetite, maghemite and, hematite (Fig. 3) [9]. Taking into account that the percentage of iron used for the manufacture of these artillery pieces was between Fe 70 wt% and Fe 80 wt% [14]. All the pieces of the battery of San Rafael, presented reductions in the Fe wt% up to Fe 20 wt%, showing structural damage and wear to the abrasion. The samples C1 % of Fe 43.18 wt%, C3 with Fe 49.12 wt%, C8 with Fe 51.76 wt% were the most affected, showing in the mouth of the barrel inside, cracks of different sizes in the metallic matrix and total or partial loss of the material, the pieces C4, C5, C6 and C7 presented of Fe 54.83 wt% values of 54.74 wt%, 52.43 wt% and 54.49 wt%, being less affected by desquamation, the piece with less wear and corrosion loss was C2 with Fe 62.94 wt%.

The Fig. 4 presents the stereoscopic microphotographs made for samples C1-C8, the difference between silica calcareous crusts, particles of marine salts and iron salts can be clearly determined. Ferrous oxide particles for samples C1, C4, C5 and C6 showed a greater tendency to aggregation and magnetization, while samples C7 and C8 showed greater particle disintegration and higher richness in marine chloride salts, perhaps due to the direction of the wind that impacts them, because of their location into San Rafael Battery. The middle zone of the pieces, reports appreciable amounts of iron oxide phases, for which reason it was selected for the analysis by confocal Raman microcopy (Fig. 3). Which also allowed to obtain more information of the phases of the oxyhydroxides present.

3.1 Study of the decomposition of the Lepidocrocite phase with relation OH-/Fe^{3+}= 0.75, using Raman laser (RLS)

Raman spectroscopy allowed a better study of Fe-OH and Fe-O binding vibrations because hydrated species do not contribute [15]. In marine saline environments, high humidity and temperature increase the rate of corrosion. In order to promote structural changes in the phases of

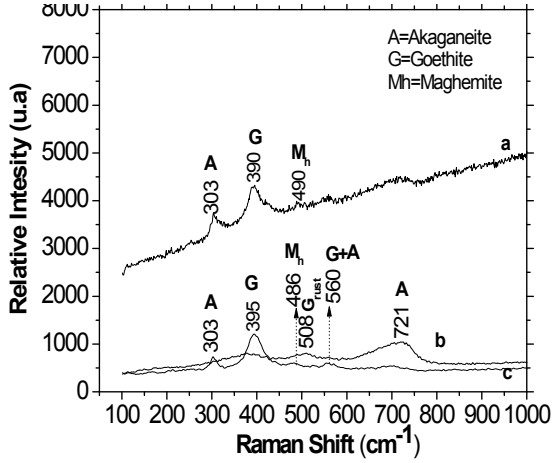

Fig. 6 Raman spectra of archaeological artefacts C1 in marine environmetal exposure; a) yellow zone b) black zone c) red zone.

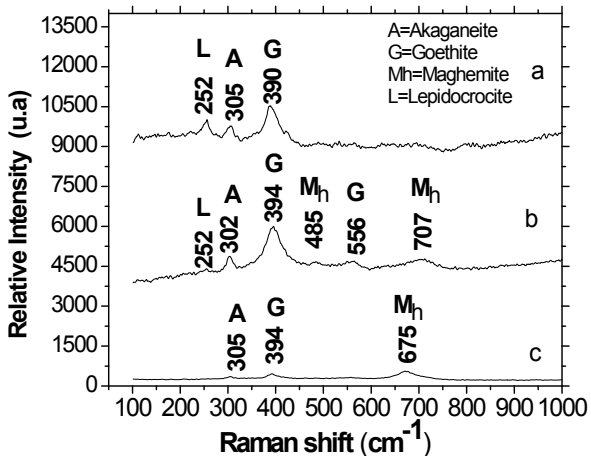

Fig. 7 Raman spectra of archaeological artefacts C2 in marine environmetal exposure; a) yellow zone b) black zone c) red zone.

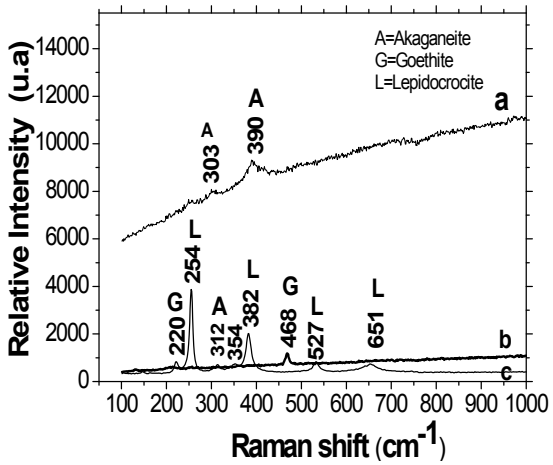

Fig. 8 Raman spectra of archaeological artefacts C3 in marine environmetal exposure; a) yellow zone b) black zone c) red zone.

synthesized lepidocrocite (Fig. 5), the charge flow in the laser was varied introducing a voltage of 1.0ev, 1.3 ev and 1.5 ev, which increased the vibrational energy of the lepidocrocite atoms, causing an increase in temperature that changed the profile of the Raman spectrum and propitious changes of the chemical environment of the dominant oxide or oxyhydroxide and other minority compounds by thermal effect [16]. It is appreciated that the synthesized phase corresponds mostly lepidocrocite (Fig. 5a), with characteristic main signals at 390 cm^{-1} and 694 cm^{-1} [17], other Raman bands at 298.4 cm^{-1}, 518.7 cm^{-1} and 1031 cm^{-1}, were related to impurities of α-FeO(OH). The low temperature produced by the 1.0v intensity, produced a slight displacement of the lepidocrocite band to 392.8 cm^{-1} (Fig. 5a) being more suitable for the analysis of this phase and avoiding acute structural changes. An intensity greater than (0.3v) (Fig. 5b), raised the temperature of the surface that made it possible to form the Fe-O-Fe bond and / or reorganization of the hydroxyl groups, generating a shift to a larger wave number of the signal characteristic of lepidocrocite at 395 cm^{-1}. With the formation of mixed phases of the goethite oxyhydroxides, with signals at 301.8 cm^{-1}, 395.4 cm^{-1} and 996.7 cm^{-1} and the band at 1048.5 cm^{-1} assigned to an unknown intermediate oxide [18]. When the laser was operated at (1.5v) (Fig. 5c), the profile of the Raman spectrum changed drastically, possibly due to the loss of structural hydroxyl present in the iron oxidohydroxides, the characteristic γ -FeO (OH) signal disappearing and facilitating the consecutive formation of oxide species as poorly crystallised hydrated iron III oxide or oxyhydroxide [18] the signal at 670.1 cm^{-1} is due to the presence of the oxidic phase, magnetite Fe_3O_4 [20], which has previously been reported as the final decomposition product of lepidocrocite. [17] the 1295.4 cm^{-1} band may be related to the phase γ -FeO(OH), while a large part of the stretches at 301.4 cm^{-1}, 395.8 cm^{-1}, 869.5 cm^{-1} and 1418.4 cm^{-1} were associated with the maghemite phase γ-Fe_2O_3 with signals of non-stoichiometric oxyhydroxides of Fe (III) [8] at 611.7 cm^{-1}, 1051.5 cm^{-1}. In none of the experiments with different intensity of the laser led to the formation of hematite α- Fe_2O_3, which is a substantial product as α-FeO (OH) and β-FeO (OH) [6]. It is postulated that the decomposition sequence suffered by the sample is γ-FeO(OH) → α-FeO(OH) + γ -FeO(OH)→ γ–Fe_2O_3+ Fe_3O_4.

3.2 Types of iron oxides associated with corrosion stages of metallic artifacts, using Raman laser (RLS)

The identification and analysis of the evolution of iron oxides and oxyhydroxides, as corrosion products, on the surface of the archaeological artifacts C1-C8, (Fig. 6 to

Fig. 13), was carried out in three head areas (black zone), medium body (yellow zone) and the tip of the canyon (red zone), these parts were unearthed and placed in aeration conditions. The purpose of the study is to obtain information to prevent the degradation of the objects, after their excavation and to have a real criterion for their restoration. The total metallic substrate (M) of the Bocachica-Colombia canyons, from this study presents the same system of layers that corrode them, as well as containing small amounts of quartz and chloride salts. In all the samples, numerous fractures were observed that had exogenous elements such as silica, chloride and calcite residues. The main iron phases were identified were: lepidocrocite γ-FeOOH with bands at 219 cm^{-1}, 252 cm^{-1} and 650 cm^{-1}, for goethite α-FeO(OH) at 300 cm^{-1}, for akaganeite β -FeO(OH) at 386 cm^{-1}; at 314 cm^{-1} and 722 cm^{-1} [12], ferroxite bands at 703.1 cm^{-1}, non-stoichiometric oxides type $Fe_{3-x}O_4$ bands were used at 532 cm^{-1} and at 667 cm^{-1}, the signal reported at the band located about 380 cm^{-1} can not be used as a criterion for the identification of any phase, because it is a superposition of the strongest bands of goethite an β - FeO (OH), and also to the following stronger bands of γ-FeO(OH) non-stoichiometric magnetite ($Fe_{3-x}O_4$), magnetic and supermagnetic goetite (α-FeOOH), lepidocrocite γ-FeO(OH) and akaganeite β-FeO(OH) [12], these were extracted from several articles [5,6,8,9,12-20, 14-15]. The studied zones of each part showed differences in the composition of the ferrous oxides, indicating a greater or lesser degree of affectation against corrosion, the Raman spectra are presented for each one of the zones separately. The metallic substrates of each metal device were heterogeneous with changes in iron composition and structure.

3.2.1 Metal artifact C1 and C2

Canyon C1 is at the end of the San Rafael Battery, faces the sky and is most affected by the winds, showing richness in the akaganeite phase and maghemite [5,6,8,9,12-20,14,15] in the central body of the artifact (Fig. 6a) and head (Fig. 6b), with high corrosion rates, for chlorides. The deeper layers (Fig. 6c), showed goetita and akaganeita [12]. This was corroborated with the confocal Raman microphotographs (Fig. 4 sample C1), from the yellow zone, (Fig. 6a), showed agglomerations of red-orange islands, smaller than 100μm in length, uniformly distributed belonging to akaganeite, together with black elongated crystals of goethite, more spherical and small red particles were related to maghemite, the clear areas correspond to the corrosion products that are being rearranged. White crystals of chloride superimposed on the oxides could be seen. It can be concluded that at the surface level, the degree of decomposition of the part is lower and can be recovered by preventive methods for its conservation. However, the impact of the aggressive atmosphere rich in chlorides within the natural environment, allows the infiltration in this part, together with the evaporation process can continue contributing to its process of corroding metal, being a cause of constant and immutable deterioration. The significant presence of the akaganeite phase is due to a high soluble chlorides concentration [12], benefiting the ionic diffusion and the increase of the electrochemical process that causes the corrosion.

The metallic device C2 located next to the C1, showed in the central zone, (Fig. 7a) akaganeita and goethite at greater depth, [12] while on the surface lepidocrocite was found. In (Fig. 7b), maghemite was identified, in greater proportion being a sign of high corrosion [22]. The deepest layers (Fig. 7c), showed goethite, akaganeita, maghemita. [5,6,8,9,12-20,14,15], the confocal Raman microphotographs (Fig. 4 sample C2), from the yellow zone (Fig. 7a), showed agglomerations of red-orange islands corresponding to akaganeite crystals, without the presence of clear areas, that could be related to little reacomodation of corrosion products and so both its corrosion state is intermediate, its intervention is more complex and the loss of the material is notorious. Black elongated goethite crystals, spherical red maghemite particles, silica crystals and white scattered crystals corresponding to chlorides are seen. Akaganeite, probably associated with iron chloride phases, was identified as an inherent part of the corrosion layer, near the metal-oxide interface [5,12], by the degree of structural damage and not only as part of the orrin layers (rust layer) formed on carbon steel in marine seaside areas.

3.2.2 Metallic artifact C3, C4 and C5

The influence of the winds that are sources of chloride, causes that both the part of center of canyon C3, (Fig. 8a) and its head, (Fig. 8b) were rich in the phase Akaganeita and lepidocrocite mainly [12]. Bands of goethite are only reported on the head (Fig. 8b) and the tip (Fig. 8c). The Raman microscopy (Fig. 4 sample C3) showed less agglomerated crystals and predominantly yellow lepidocrocite, as well as akaganeite red-orange crystals and black goethite. A greater proportion of clear zones corresponding to corrosion products that are being rearranged were observed. We can conclude that the advance of corrosion in this part is in early stages, the presence of lepidocrocite was in smaller proportion than the samples C1 and C2, corroborated with low concentration of goethite, which appears at intermediate concentrations of chloride. The metal canyon C4 device located in the

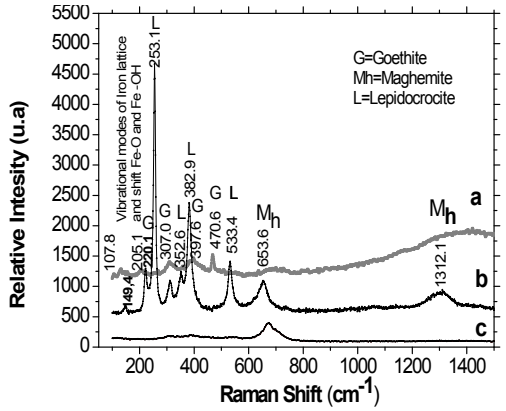

Fig. 9 Raman spectra of archaeological artefacts C4 in marine environmetal exposure; a) yellow zone b) black zone c) red zone.

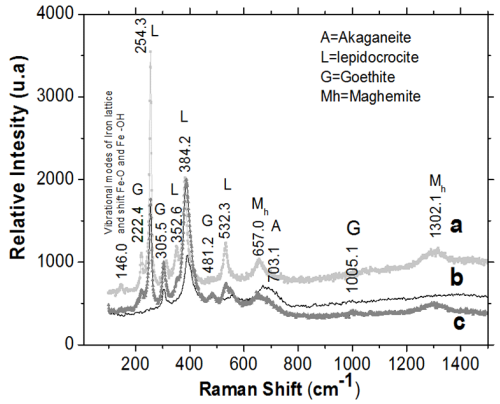

Fig. 10 Raman spectra of archaeological artefacts C5 in marine environmetal exposure; a) yellow zone b) black zone c) red zone.

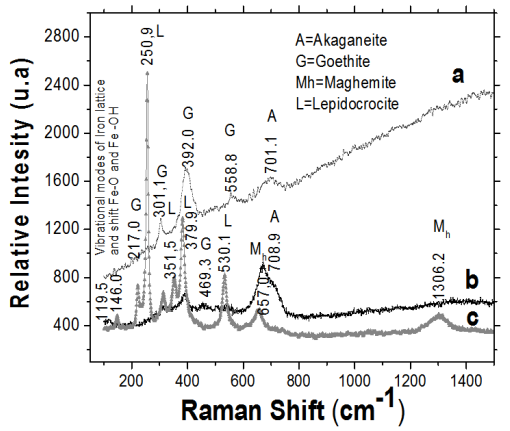

Fig. 11 Raman spectra of archaeological artefacts C6 in marine environmetal exposure; a) yellow zone b) black zone c) red zone.

center of the San Rafael Battery, (Fig. 4 sample C4), was less exposed to high chloride concentrations than C1 to C3, the center of the part its, (Fig. 9a), the head (Fig. 9b) were rich in the phase lepidocrocite, goethite and maghemite [5,6,9], the tip of the part shows a notorious disintegration of an aggressive corrosion by maghemite [23], (Fig. 9c). The increase in the crystallinity of the iron phases is noteworthy, being able to relate to the age of the part and / or the kinetics of slow formation of the protective phases of the corrosive phenomenon.

The confocal Raman microphotographs (Fig. 4 sample C4), yellow zone (Fig. 9a), showed compact red maghemite agglomerations, without clear zones representing, little reacomodation of corrosion products. Its state of corrosion is intermediate with notorious loss of material at the tip, being more difficult intervention for restorative purposes. Black elongated crystals of goethite, reddish yellow particles of lepidocrocite, transparent silica crystals and dispersed white crystals of chloride less than 1 μm are appreciated. The metallic part C5 located on the left side of C4 facing the sky (Fig. 4 sample C5), this less exposed to the chloride, the center, (Fig. 10a), the head (Fig. 10b) and the tip of the artifact, (Fig. 10c), were rich in the phase lepidocrocite, goethite, and maghemite [5-6,8-9,12], the appearance of the Raman spectrum throughout the part did not change, with intense and sharp bands of the ferrous phases present, indicating similar compositions. It is possible that there have been rearrangements at the molecular level causing the particles to grow more slowly, increasing their crystallinity, but this should be corroborated with other studies. This phenomenon could make the material more vulnerable, affecting the resistance and being a non-stick type rust. In the Raman microphotographs, (Fig. 4 sample C5), of the central yellow zone (Fig. 10a), the presence of colored crystals corresponding to ferrous oxides and oxyhydroxides, with ill-defined forms, lepidocrocite yellows, elongated blacks of goethite, reds belonging to maghemite and scattered white crystals of chloride. The corrosion process in this part is advanced and its restoration should be a priority [23].

3.2.3 Metal artifact C6, C7 and C8

The parts located at the ends of the San Rafael Battery, (Fig. 4 samples C6-C8), have greater proximity to the sea and a high contamination in chlorides, which favors the generation of akaganeite and maghemite-type phases [12], both the center of the part C6, (Fig. 11a), head (Fig. 11b) were rich in lepidocrocite, goethite showing an advanced degree of corrosion, its intervention being complex [5,6,8,9,12-20,14,15]. The Raman microscopy (Fig. 4 sample C6), from the yellow zone, (Fig. 11a), showed a compact dense structure with the presence of yellow agglomerates of lepidocrocite, red-orange goethite, brown

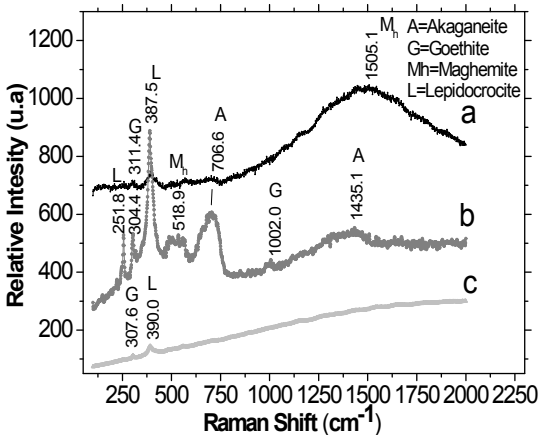

Fig. 12 Raman spectra of archaeological artefacts C7 in marine environmetal exposure; a) yellow zone b) black zone c) red zone.

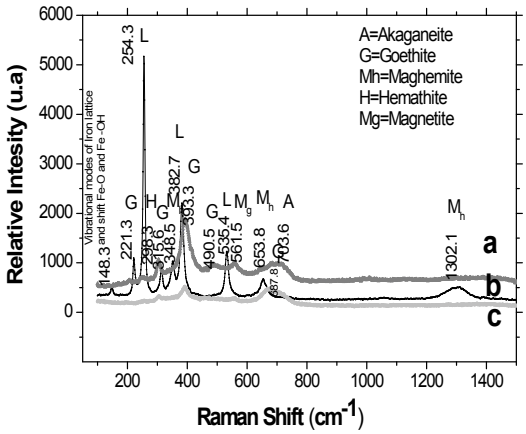

Fig. 13 Raman spectra of archaeological artefacts C8 in marine environmetal exposure; a) yellow zone b) black zone c) red zone.

maghemite coffee and elongated black crystalline forms of goethite. The appearance of white crystals, in this sample was lower than for C1 and C3. The presence of oxygen rich atmosphere, facilitated a rapid oxidation of the parts and the formation of several characteristic species of intermediate and high corrosion, that in this artifact is lost material and an advance of the disintegration of the part.

The C7 device is located with the face to the sky and at the left end of the San Rafael Battery with the complete solar radiation on the body of the device (Fig. 4 sample C7), I present in the central part, (Fig. 12a), a wide signal corresponding to the maghemite phase and it is not ruled out that this hematite, the head of the artillery artifact, (Fig. 12b), shows the most crystalline compounds being the most acute and narrow signals of the Raman spectrum, corresponding to akaganeite, goethite and lepidocrocite [5,12-14], the tip of the part (Fig. 12c) only has lepidocrocite and goethite.

The confocal Raman micrograph showed successive stages of nucleation in the formation of the oxide and oxyhydroxide phases present, a dense agglomerate structure with predominantly yellow lepidocrocite and elongated black crystals of goethite, islands of red cotton-like conglomerates can be seen maghemite Brown akaganeite crystals were much scarcer, concluding that this metallic device registers an advanced corrosion process in a rich chloride environment. The metal canyon C8 device is located at the end of the San Rafael Battery and facing the sky, (Fig. 4 samples C8), I present a profile of Raman spectrum similar to the artifacts C4 and C5. The zones studied (Fig. 13a), (Fig. 13b) and (Fig. 13c), show crystalline compounds corresponding to a non-sticky rust. With presence of lepidocrocite, goethite, akaganeite [5,12,9] in the center of the part, (Fig. 13a), the signals corresponding to 298.3 cm^{-1} related to hematite (Fe_2O_3) and 561.5 cm^{-1} would be the Fe-O vibration of the phase. magnetite (Fe_3O_4) [5,12-15]. The Raman microphotograph, (Fig. 4 sample C8), shows links of crystals of compounds such as magnetite, maghemite and goethite red and black colors, red carmine crystals of brightness corresponding to hematite, the conglomerates or islands presented magnetite or maghemite with small yellow crystals corresponding to lepidocrocite of all the archaeological artifacts studied, the most advanced degree of corrosion is highlighted with the presence of hematite and magnetite oxides of the maximum oxidation cycle of iron, whose intervention is complex for the restoration process, due to the fact that it has hematite and magnetite [14] corresponding with a highly aggressive corrosion [24].

4. Conclusions

The archaeologicals artifacts exposed to the weather, showed different iron compounds in particular in the early stage, ferric oxyhydroxides such as the lepidocrocite phase γ-FeO(OH) however, it was common to find the goethite phase α-FeO(OH) and akaganeite γ- FeO(OH) and maghemite γ-Fe_2O_3. There is evidence that the presence of lepidocrocite, goethite and akaganeite in particular at the surface level, generate less damage to the parts and can be recovered by means of preventive methods of cleaning and control of properties, for their conservation. Whereas if the product of the decomposition of themetallic material, was maghemite the phenomenon of corrosion, was aggressive and the surface of thepart is hardly recovered [25] And it is very difficult to use preventive methods for cleaning. A greater proportion of maghemite present in the parts, can lead to their breakage and loss of integrity

[14], the significant presence of the akaganeite was associated with a significant amount of soluble chlorides [12], favoring ionic diffusion by increasing the electrochemical process that causes corrosion. The high concentration of chloride suggests a strong marine influence in the corrosion process [25]. The fact that the materials are exposed to humidity and high temperatures, benefits the release of saltsthat generate cracks and fissures that become a risk for the stability and conservation of the parts. The significant presence of the akaganeite phase in the C1 canyon due to high soluble chlorides concentration [12], benefits the ionic diffusion and the increase of the electrochemical process, which is notorious in the desquamation and loss of iron in a Fe 43.18 wt%, being the part in worse condition, the C2 canyon has reached a stability in the advance of corrosion and has the highest percentage of metallic element. The C3 canyon is in an early stage of corrosion, characterized by large concentrations of lepidocrocite, but its intervention is a priority due to the rapid loss of metallic material. Cannons C4, C5 and C6 register intermediate levels of corrosion, while the most affected part in cannon 8 with partial requests for metallic crusts and highly aggressive environmental corrosion with significant presence of the hematite and magnetite.

Acknowledgments

Unicartagena- Council of Research, for grant P-2010 and 2017 FCEN. Ajover S.A Colombia Company. Chemist.Vicente Caro, for material sampling.

References

1. H. H. Uhlig. *Uhlig's Corrosion Handbook*, 2nd ed., pp. 15 - 21, John Wiley & Sons, Londres (2000).
2. T. Misawa, M. Yamashita, H. Miyuki, and H. Nagano, *Corros. Sci*., **14**, 131 (1974).
3. Z. Wang, J. Liu, and R. Han, *Corros. Sci.,* **67**, 1 (2013).
4. T. Ishikawa, K. Yhoshinori, A.Yasukawa, and K. Kazuhiko, *Corros. Sci*., **40**, 1239 (1998).
5. U. Schwertmann and R. M. Cornell, *Iron Oxides in the Laboratory*: *Preparation and Characterization*, pp. 45 - 55, VCH Publishers, Inc. Weinheim, Germany (2003).
6. H. Naono and K. Nakai, *J. Colloid Interf. Sci*, **128**, 146 (1989).
7. B. Prélot, F. Villiéras., M. Pelletier, G. Gérard, F. Gaboriaud, J. J. Ehrhardt, J. Perrone, M. Fedoroff, J. Jeanjean, G. Lefèvre, L. Mazerolles, J. L. Pastol, J. C. Rouchaud, and C. Lindecker, *J. Colloid Interf. Sci.*, **261**, 244 (2003).
8. U. Schwertmann and R. M. Taylor, *Clay. Clay Miner.*, **20**, 159 (1972).
9. A. U. Gehring and A. M. Hofmeister, *Clay. Clay Miner.*, **42**, 409 (1994).
10. K. M. Peterson, P. J. Heaney, and J. E. Post, *Chem. Geol.*, **444**, 27 (2016).
11. E. Matijevic, *Chem. Mater*. **5**, 412 (1993).
12. A. Remazeilles and P. Refait *Corros. Sci.*, **49**, 844 (2007).
13. A. L. Barbosa, E. Block, and J. J. Rouquerol, *Proc. 12th Congreso Iberoamericano de Catalisis*, p. 40, Fisocat, Chile (2010).
14. J. González-Sánchez, D. Arano-Recio, F. Bernes, and H. Mato, *Environmental Degradation of Infrastructure and Cultural Heritage in Coastal Tropical Climate,* 1st ed., pp. 183-200, Transworld Research Network, India (2009).
15. D. Neff, *Corros. Sci.*, **47**, 515 (2005).
16. T. Gao, H. Fjellvåg, and P. Norby, *J. Phys. Chem. B*, **112**, 9400 (2008).
17. F. Dubois, C. Mendibide, T. Pagnier, F. Perrard, and C. Duretref, *Corros. Sci.*, **50**, 3401 (2008).
18. M. H. Sousa, F. A. Tourinho, J. Depeyrot, G. J O. de Silva, and M. C. Lara, *J. Phys. Chem. B*, **105**, 1168 (2001).
19. R. Altobelli, I. Costa, and D. L Araújo de Faria, *Mat. Res.*, **6**, 389 (2003).
20. N. Xianghui, L. Xiaogang, D. Cuiwei, H. Yizhong, and D. He, *J. Raman Spectrosc.*, **40**, 76 (2009).
21. M. Veneranda, J. Aramendia, L. Bellot-Gurletb, P. Colomban, K. Castro, and J. M. Madariaga, *Corros. Sci.*, **133**, 68 (2018).
22. Sei J. Oh, D. C. Cook, and H. E. Townsend, *Corros. Sci.*, **4**, 1687 (1999).
23. S, Gao, B. Brown, D. Young, and M. Singer, *Corros. Sci.*, **135**, 167 (2018).
24. V. Klimas, K. Mažeika, V. Jasulaitienė, and A. Jagminas, *J. Fluorine Chem.*, **170**, 1 (2015).
25. S. Wijesinghe and T. Zixi, *Corros. Sci. Tech.,* **16**, 273 (2017).